Suppression of Parasitic Nonlinear Processes in Spontaneous Four-Wave Mixing with Linearly Uncoupled Resonators

Federico Andrea Sabattoli,[1,*] Houssein El Dirani,[2,3] Laurène Youssef,[4] Francesco Garrisi,[1] Davide Grassani,[1] Luca Zatti,[1] Camille Petit-Etienne,[4] Erwine Pargon,[4] J. E. Sipe,[5] Marco Liscidini,[1] Corrado Sciancalepore,[2,6] Daniele Bajoni,[7] and Matteo Galli[1]

[1]*Dipartimento di Fisica, Università degli Studi di Pavia, Via Bassi 6, 27100 Pavia, Italy*
[2]*Université Grenoble Alpes, CEA-LETI, 38054 Grenoble, France*
[3]*STMicroelectronics, 38926 Crolles Cedex, France*
[4]*Université Grenoble Alpes, CNRS, LTM, 38000 Grenoble, France*
[5]*Department of Physics, University of Toronto, 60 St. George Street, Toronto, Ontario M5S 1A7, Canada*
[6]*SOITEC SA, Parc technologique des Fontaines, Chemin des Franques, 38190 Bernin, France*
[7]*Dipartimento di Ingegneria Industriale e dell'Informazione, Università degli Studi di Pavia, via Ferrata 1, 27100 Pavia, Italy*

(Received 14 November 2020; accepted 23 April 2021; published 13 July 2021)

We report on a signal-to-noise ratio characterizing the generation of identical photon pairs of more than 4 orders of magnitude in a ring resonator system. Parasitic noise, associated with single-pump spontaneous four-wave mixing, is essentially eliminated by employing a novel system design involving two resonators that are linearly uncoupled but nonlinearly coupled. This opens the way to a new class of integrated devices exploiting the unique properties of identical photon pairs in the same optical mode.

DOI: 10.1103/PhysRevLett.127.033901

Nonlinear optics has been widely exploited to produce nonclassical states of the electromagnetic field. There has been a recent focus on the use of CMOS compatible materials, such as silicon and silicon nitride, which are characterized by a strong third-order optical response that can be further enhanced by the light confinement attainable in integrated microresonators [1]. With the fabrication quality and technological maturity achieved in the last decade, integrated devices based on these materials offer the promise of efficient generation of entangled photons [2–6], heralded single photons [7,8], and squeezed light [9,10].

A key third-order nonlinear process is dual-pump (DP) spontaneous four-wave mixing (SFWM), in which pump lasers at ω_1 and ω_2 are used to generate photons at $\omega_T = (\omega_1 + \omega_2)/2$. This process can be used to generate single-mode squeezed light, a central resource in the development of continuous-variable quantum computing [11]. While conventional micrometric ring resonators have been used to enhance DP SFWM [12], their multimode nature could also lead to the amplification of unwanted nonlinear phenomena, such as single-pump (SP) SFWM. This is a problem: as shown in Fig. 1(a), when working in a limited spectral range where the effect of the group velocity dispersion (GVD) is negligible, the generation of photon pairs within a target resonance at ω_T through resonant DP SFWM occurs along with two undesired SP SFWM processes. Both of these parasitic SP SFWM processes lead to the generation of two photons, with one—and only one—of them in the mode at ω_T. This acts as a source of noise, leading to a degradation of the squeezed light [10].

To quantitatively characterize these nonlinear parasitic processes, in Fig. 1(b) we plot the photon generation rates (measured as described in the Supplemental Material [13]) due to the DP SFWM and SP SFWM processes in an integrated silicon microring resonator (length 372 μm and quality factor around 6×10^4). As expected, the generation rate for the DP SFWM is unchanged as long as the product of the two pump powers is held fixed, while the generation rate of the SP SFWM processes scales quadratically with the appropriate pump powers [14]. The generation rates of the parasitic processes, given by the sum of the two SP SFWM rates, can even be 1 order of magnitude larger than the generation rate of the DP SFWM process, with a maximum signal-to-noise ratio (SNR) of only about 2 when the two pump powers are equal.

Strategies have been proposed to mitigate these parasitic processes in dual-pump experiments. In one approach, the two pump lasers are slightly detuned from resonance, such that the SP SFWM rates are suppressed [10], but with a trade-off between SNR and generation rate. Alternatively, one can use systems composed of two or more linearly coupled resonators [9] to engineer the spectral position of the resonant modes [16], with nonlinear phenomena selectively enhanced or suppressed [17]. While this method can be very effective, the suppression of the parasitic processes is limited by the achievable resonant splitting of the coupled modes [9]. Finally, dispersion engineering could be used to overcome this intrinsic limit [18], but it may impose unwanted requirements on the system, such as the need to work with optical modes separated by large spectral intervals.

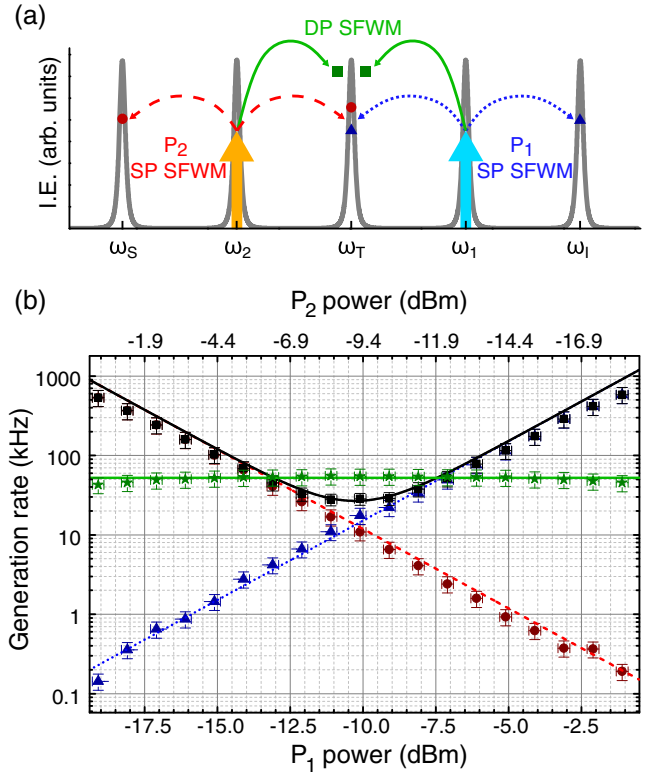

FIG. 1. (a) Sketch of the SP SFWM and DP SFWM processes occurring in a single microring resonator when two laser pumps P_1 and P_2 are aligned with two resonances (ω_1 and ω_2). If GVD can be neglected, all the processes are resonant and exploit a significant intensity enhancement (I.E.). (b) Measurement of the pair generation rate in a single silicon microring resonator when the product of the powers of the two pumps is fixed. The blue triangles and the red circles show the SP SFWM processes pumped by the lasers at ω_1 and ω_2, respectively. The black squares show the sum of the parasitic process rates, and the green stars show the DP SFWM generation rate. The measures are compared with the theoretical calculation (shown with the dotted blue line for the P_1-pumped SP SFWM, the dashed red line for the P_2-pumped SP SFWM, and the green line for the DP SFWM). See the Supplemental Material [13] for the experimental details and the theoretical calculations.

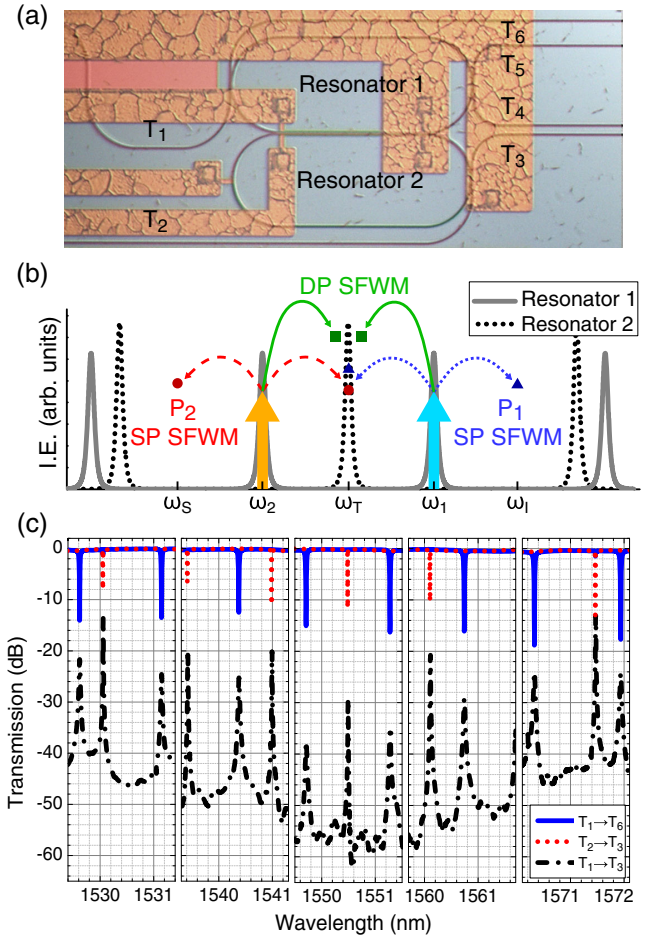

FIG. 2. (a) Optical image of the device with two linearly uncoupled racetracks. A second image of the device without the electrical circuits has been superimposed to show the position of waveguides, which are covered by the metal. (b) Sketch of the SP SFWM and DP SFWM processes occurring in the device when two laser pumps are aligned with two resonances (ω_1 and ω_2). Single-pump processes which generate photons at ω_T are suppressed due to the weak field enhancement experienced at the spectral position where energy conservation is preserved. (c) Linear characterization of the device.

In 2019, Menotti *et al.* [19] proposed a new strategy in which two linearly uncoupled optical resonators are coupled solely through the nonlinear interaction. The system is characterized by two independent sets of resonances that can be tuned to selectively enhance or suppress different nonlinear phenomena. In Fig. 2(b) we represent a sketch of the realization of DP SFWM in such a system. Two laser pumps are tuned to resonances of the first resonator, leading to the generation of photon pairs within a target resonance of the second resonator. Yet SP SFWMs are expected to be suppressed, for the overall field enhancement at $\omega_S = 2\omega_2 - \omega_T$ and $\omega_I = 2\omega_1 - \omega_T$ is strongly reduced by the absence of the three resonances satisfying energy conservation. In this Letter we experimentally demonstrate this scheme.

The device is presented in Fig. 2(a): two SOI racetrack resonators (waveguide cross section 600×220 nm^2 to optimize the nonlinear effective area and minimize propagation losses) with different lengths $\mathcal{L}_1 = 372$ μm and $\mathcal{L}_2 = 366$ μm, are located side by side, forming a directional coupler (DC) of length $L_{\mathrm{DC}} = 92$ μm, chosen to minimize cross transmission and achieve isolation of the two resonators. Thus, one set of modes is associated with resonator 1 (R_1), and another with resonator 2 (R_2). During the fabrication process, a H_2 thermal annealing was used to smooth the sidewalls of silicon waveguides [20]: this leads to a reduction of the propagation losses, and thus to a realization of resonators with high quality factors [21]. The optical characterization is shown in Fig. 2(c). The resulting two independent sets of resonances are clearly observed

by injecting light from a tunable laser in the ports T_1 or T_2 and detecting the optical response at the ports T_6 and T_3, respectively. The free spectral range at 1550 nm is around 1.566 and 1.595 nm for R_1 and R_2, respectively. The loaded quality factors are around 6×10^4 and 3×10^5, with the difference due to the different number of waveguides coupled to the racetracks (two to R_1 and one to R_2), which have the same intrinsic quality factors of about 6×10^5. The optical isolation is at least 20 dB over a 40-nm bandwidth, as observed from the transmission spectrum $T_1 \rightarrow T_3$. The two sets of resonances can be controlled independently by means of two electric heaters fabricated with a TiN layer on top of the silica cladding, and the electrical contact is realized with AlCu electric wires deposited on top of the chip.

Measurements of the nonlinear processes are realized with the experimental setup presented in Fig. 3. The light from two tunable lasers (Santec TSL710 and TSL510) is coupled using a collimator and lens to match the mode field diameter of the edge coupling tip on the chip, after two bandpass filters BPF_1 and BPF_2 (FWHM around 8 nm) have been used to filter out the amplified spontaneous emission from the lasers. The spectral position of the resonances of R_1 is controlled by using an external voltage source (Keithley 2400 Source Meter) and a multicontact wedge. The generated photon pairs are collected with a tapered fiber coupled to the port T_3 of the device, and the fiber is connected to the circulator C_1. A tunable fiber Bragg filter (TFB_1) is used in reflection [65 pm, 3 dB bandwidth, and 40 dB of extinction ratio (ER)] to route photons at frequencies around ω_T toward the detection system. Another bandpass filter (BPF_3) with more than 60 dB of ER filters out any residuals from the pump, and a fiber 50:50 beam splitter splits the photon flux toward the superconductive single-photon detectors D_1 and D_2 supplied by Photon Spot™.

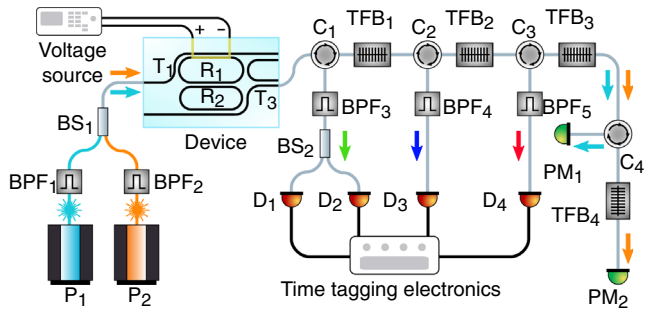

FIG. 3. Experimental setup used to measure the coincidence rates. Pump light from two lasers, combined into the same fiber through a beam splitter BS_1, is coupled to resonator R_1, the resonances of which are tuned by changing the voltage applied to the heater. Photons generated through DP SFMW and SP SFWM are collected with a tapered fiber and sorted by frequency using tunable fiber Bragg filters (TFB_1–TFB_3) and circulators (C_1–C_3). They are then detected using four superconductive single-photon detectors (D_1–D_4).

Photons at ω_T can be generated through SP SFWM only if another photon is generated to guarantee the conservation of energy. In particular, SP SFWM pumped by the laser at ω_1 (P_1 SFMW) can generate a photon pair with one photon at ω_T and one at ω_I, such that $\omega_I = 2\omega_1 - \omega_T$. Similarly, SP SFWM associated with the laser at ω_2 (P_2 SFMW) can generate one photon at ω_T and one photon at ω_S, where $\omega_S = 2\omega_2 - \omega_T$. To detect these photons, we use two tunable fiber Bragg filters (TFB_2 and TFB_3) and two bandpass filters (BPF_4 and BPF_5) to route photons at ω_I and ω_S toward superconductive single-photon detectors D_3 and D_4, respectively. Finally, the alignment of the two laser pumps is checked during the whole experiment using two power meters (PM_1 and PM_2), a circulator (C_4), and an additional bandpass filter (TFB_4).

The total insertion losses from the lasers to the waveguide coupled with R_1 at the port T_1 are around -7.8 ± 0.1 dB for the light from both P_1 and P_2. The losses from the waveguide coupled with R_1 at the port T_3 to D_1 and D_2 are around -10.7 ± 0.3 dB and -10.1 ± 0.3 dB, respectively, for the photons at ω_T; the losses from T_3 to D_3 are -11.9 ± 0.3 dB for photons at ω_I, and -7.6 ± 0.3 dB from T_3 to D_4 for photons at ω_S. The efficiency of the detectors is -1.00 ± 0.05 dB.

We begin by verifying the capability of our structure to suppress SP SFWM. To do that, we measure the variation of the efficiency of a SP SFWM process by tuning the two sets of resonances, which leads to a modification of the nonlinear coupling of the modes. We start by adjusting the voltage applied to the heater of R_1 so that the frequency ω_2 of a resonance (vacuum wavelength $\lambda_2 = 1560.916$ nm) is in the middle of the frequencies of two resonances of R_2 (at vacuum wavelengths $\lambda_T = 1550.495$ nm and $\lambda_U = 1571.479$ nm). This configuration should guarantee a maximum efficiency of P_2 SFWM since $\omega_U = \omega_S = 2\omega_2 - \omega_T$. Then, with laser P_1 turned off, we change the driving voltage of the heater of R_1 to shift its resonances, and we tune P_2 at each step to be on resonance with R_1 at each λ_2 by checking the transmission on the power meter PM_2. The tunable fiber Bragg filter TFB_1 is aligned with the resonance at ω_T at the beginning of the experiment since thermal cross talk leads to a tuning of the resonances of R_2 within the bandwidth of the filter. On the other hand, the filter TFB_2 is tuned to collect the photons generated at $\omega_S = 2\omega_2 - \omega_T$, which requires the adjustment of its spectral alignment during the entire experiment. In Fig. 4 we show the attenuation of the single-pump SFWM process with respect to the detuning of the resonances involved, which is estimated from the driving voltage and the characterization of the heater (see the Supplemental Material [13] for details). In particular, that detuning is defined as $\Delta\omega_2 - (\Delta\omega_T - \Delta\omega_U)/2$. We find that the simulation and the data are in good agreement and exhibit the expected behavior.

This result shows that by tuning the two sets of resonances one can manipulate the nonlinear coupling of

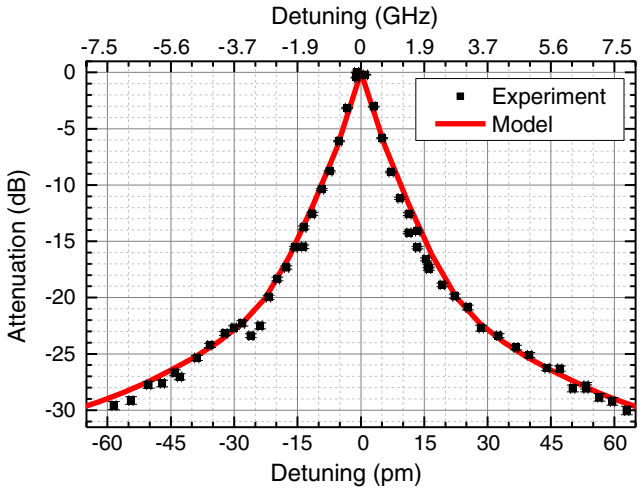

FIG. 4. Plot showing the attenuation of SP SFWM as a function of the detuning of the resonances of the two resonators.

the modes of the resonators and, consequently, the generation of pairs due to the nonlinear processes occurring in the device. In particular, a detuning of around 65 pm (8.1 GHz, around 13 times the linewidth of the resonances of R_2) leads to a suppression of around 3 orders of magnitude with respect to perfect nonlinear coupling.

With the possibility of attenuating the parasitic processes demonstrated, we proceed to the dual-pump SFWM experiment. The laser pumps are aligned with two resonances of R_1 (vacuum wavelengths $\lambda_1 = 1540.374$ nm and $\lambda_2 = 1560.742$ nm), which are equally spaced in frequency about a resonance of R_2 at $\lambda_T = 1550.491$ nm. This configuration is associated with a detuning of the SP SFWM resonances of around -160 pm (-20 GHz), and the estimation of the resulting attenuation of the SP SFWM processes is around -37.3 dB. The quality factors of the resonances of R_1 are around $Q_1 = 6.7 \times 10^4$ and $Q_2 = 5.7 \times 10^4$, while the resonance of R_2 at λ_T has a much higher quality factor, $Q_T = 3.2 \times 10^5$. We align the tunable filter TFB_1 to λ_T, while TFB_2 and TFB_3 are tuned to route photons at $\lambda_I = 1530.388$ nm and $\lambda_S = 1571.129$ nm to D_3 and D_4, respectively. The analysis of the coincidences on the detectors allows for the recognition of the pairs generated through the different processes. In particular, the DP SFMW should lead to a temporal correlation between the detection events at D_1 and D_2. Similarly, the single-pump processes should result in coincident detection: P_1 SFWM between the events at D_3 and D_1 (or D_3 and D_2), and P_2 SFWM between the events at D_4 and D_1 (or D_4 and D_2).

As discussed earlier [19], the efficiency of the DP SFWM process in our device is reduced from what could be achieved with a simple microring since here the nonlinear interaction occurs only in the directional coupler region shared by the two rings. This decreases both the overlap integral of the fields (1/4) and the interaction length ($L_{\mathrm{DC}} \approx \mathcal{L}/4$). This would be a limitation in the framework of squeezed-light sources, where high generation efficiency is required. However, a small interaction length and material nonlinearity can be compensated for by taking advantage of the field enhancement in high-quality ring resonators, and by increasing the pump intensity in the absence of nonlinear losses, as in SiN resonators [22,23].

In Fig. 5 we show the result of a coincidence experiment with the current device, where 0.95 ± 0.05 mW of optical power is coupled into the waveguide from each pump laser. The data are acquired for 20 min, and the histograms have a bin width equal to 35 ps, which is comparable to the time jitter of the detectors. The red peak shows that photons arriving on D_1 and D_2 are emitted at the same time since their arrival time is correlated: this clearly demonstrates that they are emitted through DP SFWM since any other process that can generate photons at λ_T cannot be characterized by this temporal correlation. We measure a coincidence rate equal to 164.2 ± 0.4 Hz, which corresponds to an internal generation rate in the second resonator equal to 62 ± 6 kHz, and the coincidence to accidental ratio (CAR) is 1190 ± 10. The coincidence rate is estimated by integrating the peak within the entire window (and subtracting the noise), while the CAR is measured by taking into account the FWHM of the peak (16 bins of the histogram).

From the histograms in Fig. 5 it is also possible to evaluate the photon pairs generated through SP SFWM, which lead to coincidence events between D_1 and D_2 with D_3 or D_4. As can be seen, no peaks are clearly visible. In fact, the dark counts, the noise from the environment, and other parasitic processes occurring in the setup (such as Raman emission from optical fibers) hide the signal given by time-correlated photons. This is due to the severe attenuation of the processes. Nevertheless, we can estimate

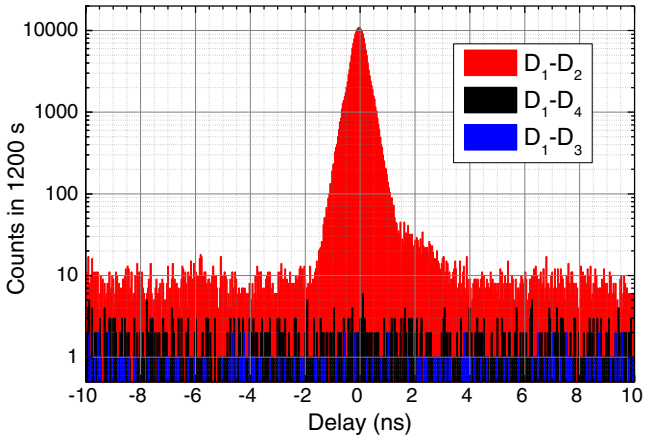

FIG. 5. Histograms representing the coincidence events detected. The red, black, and blue histograms represent, respectively, the coincidences due to DP SFWM (events on D_1 and D_2), P_2 SFWM (events on D_1 and D_4), and P_1 SFWM (events on D_1 and D_3). The delay is calculated by taking into account the different optical lengths of the fibers from the device to the detectors.

a lower bound for the SNR by analyzing the coincidences between D_1 and D_4. We integrate the peak due to DP SFWM over its FWHM (16 bins), and we divide it by the noise, which is calculated as the average on the black histogram in Fig. 5 multiplied by 16 bins. By taking into account the losses, we obtain a SNR equal to $(11.3 \pm 3.2) \times 10^3$. From the model, we should expect that the SNR is around 21×10^3, corresponding to an improvement of about 4 orders of magnitude over that of a single ring system where dispersion engineering cannot be exploited. Our experimental estimation is lower since we are overestimating the noise due to SP SFWM. While the effectiveness of this and other strategies depend critically on the specific application and the technological platform, to the best of our knowledge this is by far the strongest suppression of parasitic processes reported in the literature for DP SFWM in an integrated structure.

These results demonstrate that the use of linearly uncoupled resonators allows for the effective control of the nonlinear interaction between optical modes, leading to the ability to enhance or suppress the generation of photon pairs through spontaneous four-wave mixing. This kind of device will be a central component in strategies for the implementation of continuous-variable quantum computing. It will enable the possibility of realizing sources of highly squeezed light since the main sources of noise, due to single-pump spontaneous four-wave mixing, can be effectively suppressed. In our experiment, we could confirm the achievement of a signal-to-noise ratio of about 4 orders of magnitude.

This work has been supported by Ministero dell'Istruzione, dell'Università e della Ricerca [MIUR grant Dipartimenti di Eccellenza 2018-2022 (F11I18000680001)]. J. E. S. acknowledges support from the Natural Sciences and Engineering Research Council of Canada. The device has been designed using the open source Nazca design™ framework.

*federicoandrea.sabattoli01@ateneopv.it

[1] P. P. Absil, J. V. Hryniewicz, B. E. Little, P. S. Cho, R. A. Wilson, L. G. Joneckis, and P.-T. Ho, Opt. Lett. **25**, 554 (2000).
[2] D. Grassani, S. Azzini, M. Liscidini, M. Galli, M. J. Strain, M. Sorel, J. E. Sipe, and D. Bajoni, Optica **2**, 88 (2015).
[3] N. C. Harris, D. Grassani, A. Simbula, M. Pant, M. Galli, T. Baehr-Jones, M. Hochberg, D. Englund, D. Bajoni, and C. Galland, Phys. Rev. X **4**, 041047 (2014).
[4] J. W. Silverstone, R. Santagati, D. Bonneau, M. J. Strain, M. Sorel, J. L. O'Brien, and M. G. Thompson, Nat. Commun. **6**, 7948 (2015).
[5] M. Kues, C. Reimer, P. Roztocki, L. R. Cortés, S. Sciara, B. Wetzel, Y. Zhang, A. Cino, S. T. Chu, B. E. Little, D. J. Moss, L. Caspani, J. Azaña, and R. Morandotti, Nature (London) **546**, 622 (2017).
[6] P. Imany, J. A. Jaramillo-Villegas, O. D. Odele, K. Han, D. E. Leaird, J. M. Lukens, P. Lougovski, M. Qi, and A. M. Weiner, Opt. Express **26**, 1825 (2018).
[7] X. Lu, S. Rogers, T. Gerrits, W. C. Jiang, S. W. Nam, and Q. Lin, Optica **3**, 1331 (2016).
[8] Y. Liu, C. Wu, X. Gu, Y. Kong, X. Yu, R. Ge, X. Cai, X. Qiang, J. Wu, X. Yang, and P. Xu, Opt. Lett. **45**, 73 (2020).
[9] Y. Zhang, M. Menotti, K. Tan, V. D. Vaidya, D. H. Mahler, L. Zatti, M. Liscidini, B. Morrison, and Z. Vernon, Nat. Commun. **12**, 2233 (2021).
[10] Y. Zhao, Y. Okawachi, J. K. Jang, X. Ji, M. Lipson, and A. L. Gaeta, Phys. Rev. Lett. **124**, 193601 (2020).
[11] Z. Vernon, N. Quesada, M. Liscidini, B. Morrison, M. Menotti, K. Tan, and J. E. Sipe, Phys. Rev. Applied **12**, 064024 (2019).
[12] Y. Guo, W. Zhang, S. Dong, Y. Huang, and J. Peng, Opt. Lett. **39**, 2526 (2014).
[13] See Supplemental Material at http://link.aps.org/supplemental/10.1103/PhysRevLett.127.033901, which includes Refs. [14] and [15], for the details about the single-resonator nonlinear experiment, and the estimation of the detuning of the resonances of the linearly uncoupled resonators.
[14] L. G. Helt, M. Liscidini, and J. E. Sipe, J. Opt. Soc. Am. B **29**, 2199 (2012).
[15] S. Azzini, D. Grassani, M. Galli, L. C. Andreani, M. Sorel, M. J. Strain, L. G. Helt, J. E. Sipe, M. Liscidini, and D. Bajoni, Opt. Lett. **37**, 3807 (2012).
[16] C. M. Gentry, X. Zeng, and M. A. Popović, Opt. Lett. **39**, 5689 (2014).
[17] M. Heuck, J. G. Koefoed, J. B. Christensen, Y. Ding, L. H. Frandsen, K. Rottwitt, and L. K. Oxenlowe, New J. Phys. **21**, 033037 (2019).
[18] B. Fang, O. Cohen, V. O. Lorenz, and J. B. Moreno, Opt. Express **21**, 2707 (2013).
[19] M. Menotti, B. Morrison, K. Tan, Z. Vernon, J. E. Sipe, and M. Liscidini, Phys. Rev. Lett. **122**, 013904 (2019).
[20] C. Bellegarde, E. Pargon, C. Sciancalepore, C. Petit-Etienne, V. Hugues, D. Robin-Brosse, J.-M. Hartmann, and P. Lyan, IEEE Photonics Technol. Lett. **30**, 591 (2018).
[21] F. A. Sabattoli, H. El Dirani, F. Garrisi, S. Sam, C. Petit-Etienne, J. M. Hartmann, E. Pargon, C. Monat, M. Liscidini, C. Sciancalepore, M. Galli, and D. Bajoni, in *Proceedings of the 21st International Conference on Transparent Optical Networks (ICTON)* (2019), pp. 1–4.
[22] H. El Dirani, L. Youssef, C. Petit-Etienne, S. Kerdiles, P. Grosse, C. Monat, E. Pargon, and C. Sciancalepore, Opt. Express **27**, 30726 (2019).
[23] M. H. P. Pfeiffer, J. Liu, A. S. Raja, T. Morais, B. Ghadiani, and T. J. Kippenberg, Optica **5**, 884 (2018).